19. M. Capogna, B. H. Gahwiler, S. M. Thompson, *J. Neurophysiol.* **76**, 3149 (1996).
20. G. Lonart *et al.*, *Neuron* **21**, 1141 (1998).
21. M. Geppert *et al.*, *Cell* **79**, 717 (1994).
22. Western blot analysis. RGC cell lysates were prepared by extraction with 2% SDS. Proteins were resolved by SDS–polyacrylamide gel electrophoresis and transferred onto polyvinylidene difluoride (Millipore). Membranes were incubated in blocking buffer [phosphate-buffered saline (PBS) containing 0.1% Tween-20 and 5% nonfat milk] for 30 min at room temperature, followed by incubation for 1 hour in blocking buffer containing either affinity-purified rabbit antibodies to synaptotagmin lumenal domain (1.0 μg/ml), mouse anti-synaptophysin (1:1000; Sigma), or mouse anti-p115 (1:2000) (provided by M. G. Waters, Princeton University). Immunoreactive proteins were detected with horseradish peroxidase (HRP)–conjugated anti-rabbit or anti-mouse immunoglobulin G (1:40,000; Jackson Immunoresearch) and visualized with a chemiluminescent substrate for HRP (SuperSignal West Pico, Pierce Chemicals).
23. Immunocytochemistry. RGC cultures were fixed in 4% paraformaldehyde in PBS or phosphate buffer (pH 7.4) for 5 min at room temperature and washed in PBS containing 0.3% Triton X-100. Primary antibodies were applied at various concentrations overnight in staining buffer [0.5% bovine serum albumin, 0.5 % Triton X-100, 30 mM $NaPO_4$ (pH 7.4), 750 mM NaCl, 5% normal goat serum, and 0.4% NaN_3]. Secondary antibodies, goat anti-mouse and anti-rabbit Alexa 488 and Alexa 594 conjugates (Molecular Probes), were used at a dilution of 1:200 for 1 hour at room temperature. All washes were done with PBS containing 0.1% Triton X-100.
24. Target SC neurons were purified as described (*6*). Briefly, SC neurons were dissociated in papain, and microglia, macrophages, and oligodendrocytes were removed by panning with the Griphonia Symplicifolia lectin 1 (Vector Labs) and the O4 antibody. Neurons were then selected with an ASCS4 monoclonal antibody (DSHB).
25. Supplementary data are available on *Science* Online at www.sciencemag.org/cgi/content/full/291/5504/657/DC1.
26. P. G. Haydon, P. Drapeau, *Trends Neurosci.* **18**, 196 (1995).
27. S. E. Ahmari, J. Buchanan, S. J. Smith, *Nature Neurosci.* **3**, 445 (2000).
28. H. V. Friedman *et al.*, *Neuron* **27**, 57 (2000).
29. T. Schikorski, C. F. Stevens, *J. Neurosci.* **17**, 5858 (1997).
30. Electron microscopy. Cells were prepared for EM as described (*6*). Briefly, cells were washed in 0.1 M phosphate buffer (pH 7.2), then fixed for 30 min in 2% glutaraldehyde buffered with 0.1 M sodium phosphate (pH 7.2) at 4°C. After rinsing with buffer, specimens were stained en bloc with 2% aqueous uranyl acetate for 15 min, dehydrated in ethanol, and embedded in poly/bed812 for 24 hours. Fifty-nanometer sections were poststained with uranyl acetate and lead citrate and viewed with a Philips Electronic Instruments CM-12 transmission electron microscope.
31. R. D. Lund, J. S. Lund, *Brain Res.* **42**, 1 (1972).
32. S. S. Warton, R. McCart, *Synapse* **3**, 136 (1989).
33. Reversal experiments. RGCs were cultured with glia for 5 days, after which the glia were removed and the media exchanged for fresh media. Control RGCs were recorded after 5 days of coculture with glia and exchange of media for astrocyte-conditioned media.
34. J. E. Bottenstein, G. H. Sato, *J. Neurosci.* **76**, 514 (1979).
35. We thank E. Kavalali for advice on FM1-43 experiments, J. Waters and P. De Koninck for critically reading a draft of the manuscript, and M. Hernandez for technical assistance. Supported by a Mcknight Investigator Award (B.A.B.), a Kirsch Investigator Award from the Steven and Michele Kirsch Foundation (B.A.B.), and NIH grant NS10784 (E.M.U.).

18 September 2000; accepted 26 December 2000

REPORTS

Backward Spreading of Memory-Retrieval Signal in the Primate Temporal Cortex

Yuji Naya,[1]* Masatoshi Yoshida,[2]* Yasushi Miyashita[1,2,3]†

Bidirectional signaling between neocortex and limbic cortex has been hypothesized to contribute to the retrieval of long-term memory. We tested this hypothesis by comparing the time courses of perceptual and memory-retrieval signals in two neighboring areas in temporal cortex, area TE (TE) and perirhinal cortex (PRh), while monkeys were performing a visual pair-association task. Perceptual signal reached TE before PRh, confirming its forward propagation. In contrast, memory-retrieval signal appeared earlier in PRh, and TE neurons were then gradually recruited to represent the sought target. A reasonable interpretation of this finding is that the rich backward fiber projections from PRh to TE may underlie the activation of TE neurons that represent a visual object retrieved from long-term memory.

Encoding and retrieval of declarative memory depends on the integrity and interaction between the neocortex and the medial temporal lobe system (*1, 2*). The inferior temporal (IT) cortex, which serves as the storehouse of visual long-term memory (*3–10*), consists of two cytoarchitectonically distinct but mutually interconnected areas (*11, 12*): area TE (TE) and the perirhinal cortex (PRh). TE is located at the final stage of the ventral visual pathway (Fig. 1A) (*13, 14*), whereas PRh is a limbic polymodal association area (*1, 2*). Forward flow of visual information from TE to area 36 (A36), an immediate adjoining region in PRh, is thought to serve the memory-encoding process (*5, 6, 15, 16*). Recently, we found that memory neurons are more abundant in PRh (*16*), and that a neurotrophin, BDNF (brain-derived neurotrophic factor), was selectively induced in PRh during memory formation (*17*), further supporting the hypothesis of memory storage by neural circuit reorganization. However, the function of the rich backward projection from A36 to TE has not been examined. On the basis of previous observations that IT neurons are dynamically activated by the necessity for memory recall in monkeys (*18–20*), we hy-

[1]Laboratory of Cognitive Neuroscience, National Institute for Physiological Sciences, Okazaki, Aichi 444-8585, Japan. [2]Mind Articulation Project, International Cooperative Research Project (ICORP), Japan Science and Technology Corporation, Yushima, Tokyo 113-0034, Japan. [3]University of Tokyo School of Medicine, Hongo, Tokyo 113-0033, Japan.

*These authors contributed equally to this report.
†To whom correspondence should be addressed. E-mail: yasushi_miyashita@m.u-tokyo.ac.jp

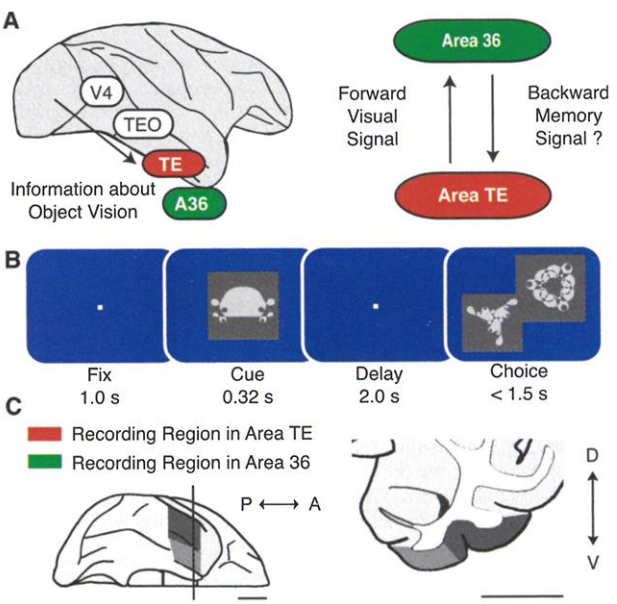

Fig. 1. (**A**) Left panel: Lateral view of a macaque brain. TE is located at the final processing stage of the ventral visual pathway. A36 is thought to be a part of the medial temporal lobe memory system. V4, visual area 4; TEO, area TEO. Right panel: Role of the backward connection from A36 to TE. A36 receives forward visual signal from TE. (**B**) Sequence of events in a trial of the PA task. Fixation points and cue stimuli were presented at the center of a video monitor. Choice stimuli were presented randomly in two of four positions on the video monitor. (**C**) Location of recording sites in TE (red) and A36 (green). Left panel: Ventral view of a monkey brain (anterior at the right). Right panel: A part of the coronal cross section (dorsal at the top) indicated by a horizontal line on the ventral view. Scale bars, 10 mm.

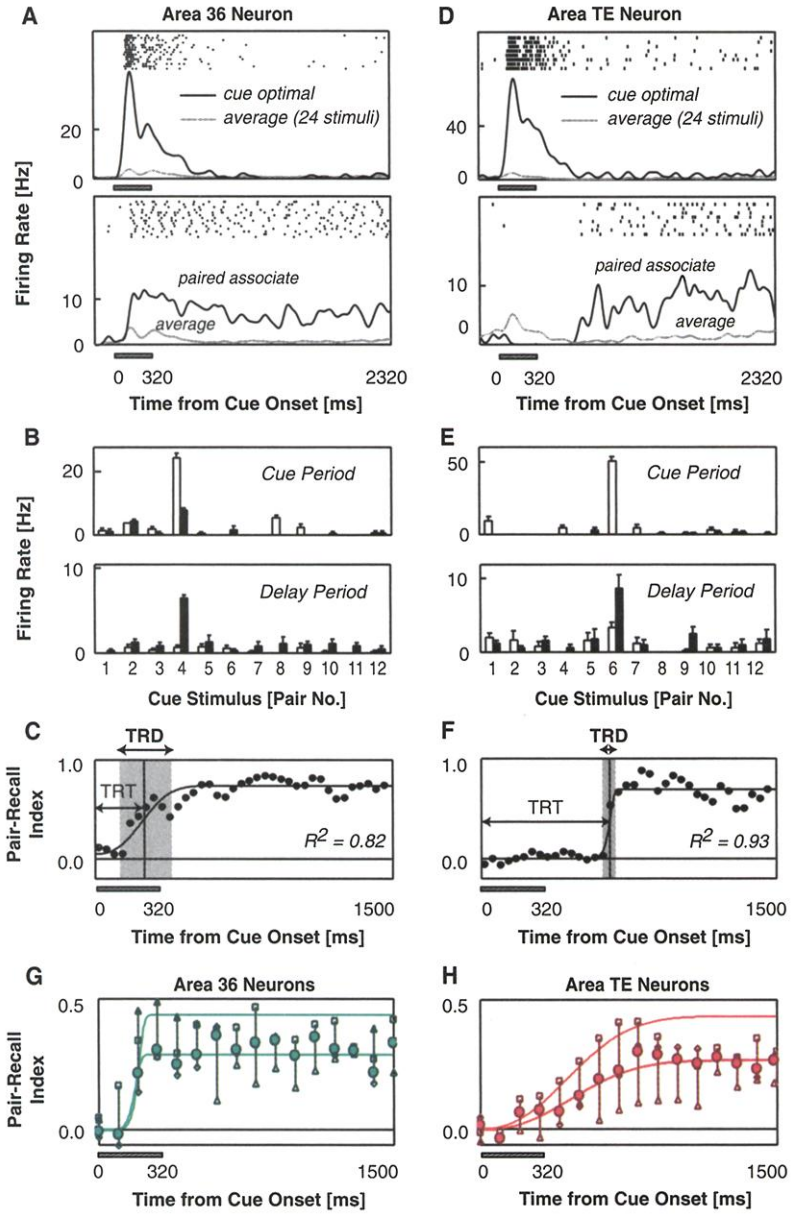

Fig. 2. Neuronal activity related to memory retrieval during the PA task, as shown by a single cell in A36 (**A** to **C**) and in TE (**D** to **F**). For the raster displays [(A) and (D)], spike density functions (SDFs) were aligned at the cue onset in trials with the cue-optimal stimulus as a cue (upper panel) and in trials with its paired associate as a cue (lower panel). In the SDFs, black lines indicate responses to the cue-optimal stimulus (upper panel) or its paired associate (lower panel), and gray lines indicate mean responses to all 24 stimuli. In (B) and (E), mean discharge rates during the cue (upper panel) and delay (lower panel) periods are shown for each cue presentation (mean ± SEM). Twelve pairs of stimuli are labeled on the abscissa. The open and filled bars in pair 1 refer to the responses to the stimulus 1 and 1′, respectively. A stimulus-selective delay activity was closely coupled with a strong cue response to its paired associate. In (C) and (F), temporal dynamics of response correlation are shown; the values of the pair-recall index (PRI) are plotted against the time axis and are fitted with Weibull functions (solid lines) (*29*). The vertical lines, intersecting the best-fit Weibull functions, indicate the transition times (TRTs). The shaded areas indicate the transition durations (TRDs). (**G** and **H**) Temporal dynamics of averaged PRI(t) for the population of the stimulus-selective neurons. Mean values of PRI(t) were plotted every 100 ms for A36 neurons [(G), green] and TE neurons [(H), red] (filled circle, total; open diamond, monkey 1; open square, monkey 2; open triangle, monkey 3). Thick lines (green and red, respectively) indicate the best-fit Weibull functions for the population-averaged PRI(t) in the two areas (A36, TRT, 181 ms, TRD, 76 ms; TE, 493 ms, 602 ms). Thin lines, same but for the neurons whose PRI(t) increased above the 5% significance level (A36, 197 ms, 69 ms; TE, 472 ms, 625 ms).

pothesized that the backward projection participates in memory-retrieval processes.

Monkeys were trained in the pair-association (PA) task (*21*), which requires retrieval of a target from long-term memory (Fig. 1B), and extracellular spike discharges of single neurons were recorded from A36 and TE (Fig. 1C) (*22*). The responses of a representative A36 neuron, with stimulus-selective delay activity related to the sought target specified by a cue stimulus (*18, 19*), are shown in Fig. 2, A to C. One stimulus elicited the strongest response during the cue period, and the response continued into the delay period (Fig. 2A, upper panel). In the trial when the paired associate of this cue-optimal stimulus was used as a cue, the same cell started to respond during the cue period without an initial perceptual response and maintained a tonic activity until choice stimuli were presented (Fig. 2A, lower panel). The paired associate elicited the highest delay activity among the stimuli (Fig. 2B). We refer to this type of activity as target-related (*19*). In TE, we also found neurons exhibiting the target-related delay activity (Fig. 2, D to F). However, the time course of the delay activity was different from that for the A36 neuron shown in Fig. 2, A to C: Although the paired associate eventually elicited the highest delay activity (Fig. 2E, lower panel), the onset of the target-related tonic activity was later than that of the A36 neuron (Fig. 2D, lower panel). We examined the time course of the target-related delay activity of each neuron by considering responses to all cue stimuli: The partial correlation coefficients of instantaneous firing rates at time t for each cue stimulus were calculated with the visual responses to its paired-associate stimulus (pair-recall index; PRI) (*23–25*). In Fig. 2, C and F, PRI(t)s for both of the neurons are plotted as a function of time; the PRI(t) for the A36 neuron started to increase earlier than that for the TE neuron.

In total, 516 visually responsive cells were recorded from A36 (123 cells) and TE (393 cells), and 418 of 516 cells were cue selective (97 cells in A36, 321 cells in TE). Of the 418 cells, 114 (45 cells in A36, 69 cells in TE) showed significant stimulus-selective activity [analysis of variance (ANOVA), $P < 0.01$] during the delay as well as during the cue period (*26*) and are referred to here as stimulus-selective neurons. First, we examined the perceptual signal and found that the latencies of visual response for these neurons in TE were significantly shorter than those in A36 (TE, median 77 ms; A36, median 89 ms; Kolmogorov-Smirnov test, $P < 0.05$) (*27*). Second, we examined the mnemonic signal. The time courses of the average PRI(t) across the population of stimulus-selective neurons in A36 and TE, respectively (Fig. 2, G and H), significantly differed between the two areas (repeated-measures ANOVA, $P < 0.0001$), which was also confirmed in all the animals ($P < 0.0001$ in monkeys 1 and 3, $P < 0.002$ in monkey 2) (*28*). The PRI(t) for the A36 neurons began to increase within the cue

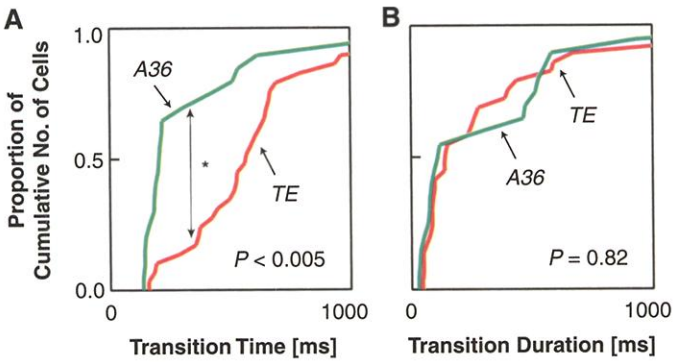

Fig. 3. Time courses of PRI(t) for single neurons. (**A** and **B**) Cumulative frequency histograms of the TRT (A) and the TRD (B) for A36 (green) and TE (red) neurons. TRTs for A36 neurons were significantly shorter than those for TE neurons (asterisk, Kolmogorov-Smirnov test, $P < 0.005$).

period and developed with a rapid time course. The PRI(t) for the TE neurons increased slowly and reached a plateau at the middle of the delay period. The slow, gradual increase of the population-averaged PRI(t) in the TE neurons could be due to the slow development of the PRI curve for single neurons, or to the wide distribution of the onset time for the PRI(t) increase.

We thus determined two parameters that characterized the time course of PRI(t) for each single neuron on the basis of the best-fit Weibull function (Fig. 2, C and F) (*29–31*). Transition time (TRT) was defined as the period from the cue onset to the instant when the Weibull function reached 50% of its full increase. Transition duration (TRD) was defined as the duration between the instants when the function reached 10% and 90% of its full increase. The parameters were definable for the stimulus-selective neurons with significantly increased PRIs (A36, $n = 20$; TE, $n = 29$) (*29*) and were compared between the two areas (Fig. 3, A and B). The TRT values for the A36 neurons were significantly shorter than those for the TE neurons (A36, median 206 ms; TE, median 570 ms; Kolmogorov-Smirnov test, $P < 0.005$; Fig. 3A) (*32*). Moreover, the shorter 70% of TRT values of the A36 neurons were distributed in the range of 138 to 304 ms (i.e., within a 166-ms time window), whereas those of the TE neurons widely ranged from 161 ms to 653 ms (i.e., within a 492-ms time window). The distributions of the TRD values did not differ between the two areas (A36, median 115 ms; TE, median 145 ms; $P > 0.8$; Fig. 3B) (*32*). These results indicate that the gradual increase in the population-averaged PRI(t) curve for the TE neurons was due to the wide distribution of TRT values for single neurons, and not due to the longer TRDs.

We examined the time course of visual and memory-retrieval signals in two subareas of IT cortex while monkeys attended to and retrieved the paired associate of the cue stimulus from long-term memory. The visual signal reached TE before it reached A36. In contrast, the memory-retrieval signal emerged earlier in A36 (median TRT, 206 ms), and TE neurons were then gradually recruited to represent the sought target (median TRT, 570 ms), although there was some overlap in the distributions of TRTs between the two areas. Interestingly, TRD did not differ between the two areas, suggesting that the neural dynamics for the growth of the memory-retrieval signal was similar in A36 and TE (*33*).

Previous studies have provided some anatomical and behavioral evidence on the nature of the memory-retrieval signals observed in the two areas, although there is as yet no direct evidence concerning which brain region effects the choice decision in the task (*30, 31*). First, area TE receives numerous backward fiber projections from A36 (*1, 2, 12, 34*). Second, two research groups have demonstrated a dissociation between the effects of damage to PRh (i.e., A36 plus A35) and damage to TE (*35, 36*). They suggested, that PRh is engaged in mnemonic processing and/or in processing stored knowledge of objects, whereas TE functions specifically in perceptual processing and/or processing structural attributes of objects. Therefore, it is a reasonable interpretation of the difference in TRT distributions in the two areas, although it is not a logical requirement, that the mnemonic signal of the target is spreading backward from A36 to TE. We cannot exclude the possibility that the delayed activations of TE neurons were generated from fast changes in other TE neurons. Another interpretation is that the delayed activations were triggered from other areas such as the prefrontal cortex. Previously, we demonstrated a top-down memory-retrieval signal from prefrontal cortex to IT cortex (*37, 38*). It remains to be clarified whether the memory-retrieval signal that TE neurons represent originates from a frontotemporal top-down signal for voluntary recall, from a limbic-neocortical backward signal for automatic recall, or from both sources depending on the demand.

References and Notes

1. R. Squire, S. Zola-Morgan, *Science* **253**, 1380 (1991).
2. M. Mishkin *et al.*, *Philos. Trans. R. Soc. London Ser. B* **352**, 1461 (1997).
3. J. M. Fuster, *Memory in the Cerebral Cortex* (MIT Press, Cambridge, MA, 1995).
4. N. K. Logothetis, D. L. Sheinberg, *Annu. Rev. Neurosci.* **19**, 577 (1996).
5. Y. Miyashita, *Annu. Rev. Neurosci.* **16**, 245 (1993).
6. _____, T. Hayashi, *Curr. Opin. Neurobiol.* **10**, 187 (2000).
7. E. A. Murray, D. Gaffan, M. Mishkin, *J. Neurosci.* **13**, 4549 (1993).
8. T. Orlov *et al.*, E. Zohary, *Nature* **404**, 77 (2000).
9. R. W. Doty, J. L. Ringo, J. D. Lewine, *Behav. Brain Res.* **64**, 79 (1994).
10. L. Schacter, R. L. Buckner, *Neurobiol. Learn. Mem.* **70**, 275 (1998).
11. W. A. Suzuki, D. G. Amaral, *J. Comp. Neurol.* **350**, 497 (1994).
12. K. S. Saleem, K. Tanaka, *J. Neurosci.* **16**, 4757 (1996).
13. K. Tanaka, *Annu. Rev. Neurosci.* **19**, 109 (1996).
14. P. Janssen, R. Vogels, G. A. Orban, *Science* **288**, 2054 (2000).
15. Z. Liu, B. J. Richmond, *J. Neurophysiol.* **83**, 1677 (2000).
16. Y. Naya *et al.*, paper presented at the 29th annual meeting of the Society for Neuroscience, Miami Beach, FL, 25 October 1999.
17. W. Tokuyama, H. Okuno, T. Hashimoto, Y. X. Li, Y. Miyashita, *Nature Neurosci.* **3**, 1134 (2000).
18. K. Sakai, Y. Miyashita, *Nature* **354**, 152 (1991).
19. Y. Naya, K. Sakai, Y. Miyashita, *Proc. Natl. Acad. Sci. U.S.A.* **93**, 2664 (1996).
20. V. Yakovlev *et al.*, *Nature Neurosci.* **4**, 310 (1998).
21. The procedure for the PA task was as described (*18, 19*). In each trial, one cue stimulus and then two choice stimuli, the paired associate of the cue stimulus (target) and one from a different pair (distractor), were sequentially presented with a delay of 2000 ms. The monkey obtained fruit juice as a reward for correctly touching the target. The visual stimuli were 24 monochrome Fourier descriptors extending approximately 5° × 5°. Eye movements were monitored with a PC-based charge-coupled device camera system, and if the eye position deviated more than 1° to 1.5° from the center of the screen, the trial was automatically terminated. The performance of each monkey was better than 90% correct.
22. Three adult monkeys (*Macaca fuscata*) were used. Head bolts and a chamber for microelectrode recording were attached to the skull under aseptic conditions and general anesthesia with sodium pentobarbital (25 mg per kilogram of body weight per hour, intravenously). Extracellular discharges of single neurons were recorded with a glass-insulated tungsten microelectrode (*19*) from one hemisphere in each monkey. Electrode placement into A36 and TE was guided by constructing individual brain atlases from MRI scans. Each location of the electrode track was measured by x-ray images. After the experiments, the recording sites were histologically reconstructed on the basis of three or four electrolytic-marking lesions and two or three injected dyes. The border between TE and A36 was determined by cytoarchitecture (*11, 12*). There was a clear separation between layers V and VI in TE but not in A36, and layer II was thicker in TE than in A36.
23. A partial correlation analysis was used to evaluate the temporal dynamics of response correlation with the target to be retrieved. The instantaneous firing rate (IFR) was defined as the mean discharge rate during the 100-ms window ending at the given time point stepped by 5 ms for each stimulus. When the stimulus i was presented as a cue, the IFR at the time t from cue onset was denoted as $f_i(t)$. The IFR to the set of 24 stimuli was denoted as a 24-dimensional vector $\mathbf{F}(t)$: $[f_1(t), \ldots, f_{24}(t)]$. The cue responses were denoted as c_i or $c_{p(i)}$ when the stimulus i or its paired associate $p(i)$ was presented as a cue, and were denoted as a vector $\mathbf{C}$: $[c_1, \ldots, c_{24}]$ or $\mathbf{Cp}$: $[c_{p(1)}, \ldots, c_{p(24)}]$. To remove the influence of correlation between the cue responses of the same pairs, we calculated partial correlations of $\mathbf{F}(t)$ with the cue responses to the paired-associate stimuli $\mathbf{Cp}$, using standard formulae (*24, 25*)

$$\mathrm{PRI}(t) = [\langle \mathbf{Cp} \mid \mathbf{F}(t) \rangle - \langle \mathbf{C} \mid \mathbf{Cp} \rangle \langle \mathbf{C} \mid \mathbf{F}(t) \rangle] / \{[1 - \langle \mathbf{C} \mid \mathbf{F}(t) \rangle]^2 [1 - \langle \mathbf{C} \mid \mathbf{Cp} \rangle]^2\}^{1/2}$$

where $\langle \mathbf{A} | \mathbf{B} \rangle$ indicates the simple correlation coefficient between **A** and **B**. Intuitively, PRI(t) represents

the correlation between **F**(t) and **Cp** when the linear effect of **C** was removed from **F**(t) and **Cp**. This measure is useful, because an IT neuron has a tendency to encode both of the paired stimuli ("pair-coding" effect) (*18, 25, 34*) and because this correlation between **C** and **Cp** must be removed in the multiple regression analysis of **F**(t). Neural discharges of IT cells reflect the cognitive demand of the PA task, and stimulus-selective delay activities are closely coupled with a strong cue response to its paired associate. This property of the delay discharges is now known as "target-related" or "prospective" signals (*18, 19, 25*). PRI(t) is influenced by weak responses if the stimulus selectivity of the neuron is rather broad, but not heavily if the stimulus selectivity is sharp, as in the case of the neuron shown in Fig. 2. PRI(t)s were fitted with cumulative Weibull functions [see text and (*29*)] by using the data stepped by 5 ms as stated above; however, for convenience, the data were plotted every 40 ms in Fig. 2, C and F, and plotted every 100 ms in Fig. 2, G and H.

24. J. A. Movshon, W. T. Newsome, *J. Neurosci.* **16**, 7733 (1996).
25. C. A. Erickson, R. Desimone, *J. Neurosci.* **19**, 10404 (1999).
26. The stimulus selectivity during the cue period (60 to 320 ms from cue onset) and the delay period (1320 to 2320 ms from cue onset) was tested by a one-way ANOVA ($P < 0.01$). All the delay-selective neurons were also cue-selective in both A36 and TE. The numbers of selective cells were 40 (TE) and 32 (A36) in monkey 1, 15 (TE) and 8 (A36) in monkey 2, and 14 (TE) and 5 (A36) in monkey 3. The proportion of delay-selective neurons in relation to cue-selective neurons (A36, 45/97; TE, 69/321) was significantly higher in A36 than in TE (χ^2 test, df = 1, $P < 0.001$).
27. Spike trains were smoothed by convolution with a Gaussian kernel (σ = 10 ms) to obtain the spike density function (SDF). The baseline activity was defined as the mean discharge rate during the 300-ms period just preceding cue onset. The latency of the neuronal response was determined as the time point when the SDF for the optimal stimulus first exceeded a level +2 standard deviations from the baseline activity.
28. A repeated-measures ANOVA (Area × Time × Animal) was used to compare the time courses of PRI(t) for the population of stimulus-selective neurons (subject factor; neurons, df = 108) in each area (between-subject factor; Area, df = 1) of each animal (between-subject factor; Animal, df = 2) at each time point (t = 0, 100, ..., 2300 ms) (within-subject factor; Time, df = 23). The interaction between Area and Time indicated significant difference in the time course between the two areas ($P < 0.0001$). There was neither a main effect of Animal ($P > 0.12$) nor an interaction among Area, Time, and Animal ($P > 0.084$). The time course of the PRI(t) in each animal was also examined by a repeated-measures ANOVA (Area × Time). The interactions between Area and Time were significant in all the animals ($P < 0.0001$, $P < 0.002$, $P < 0.0001$, respectively).
29. To characterize the growth in PRI(t) with time, we fitted the data with a cumulative Weibull function (*30, 31*)

$$W(t) = \gamma - (\gamma - \delta) \cdot \exp[-(t/\alpha)^{\beta}]$$

where γ is the maximum value, δ is the minimum value, t is the time after cue presentation, α is the time point at which the curve reaches 64% of its full growth, and β is the slope in the PRI. The best-fit Weibull function was determined by using the data after cue onset. Among the 114 stimulus-selective neurons, TRT and TRD were determined for the stimulus-selective neurons whose best-fit Weibull function for the PRI(t) increased above the 5% significance level ($r = 0.352$, df = 21). The best-fit Weibull curves accurately represented the PRI change with time for these neurons as judged by the R^2 values (R^2 = 0.35 to 0.95, mean 0.66).
30. S. Celebirini, W. T. Newsome, *J. Neurosci.* **14**, 4109 (1994).
31. K. G. Thompson *et al.*, *J. Neurophysiol.* **76**, 4040 (1996).
32. A two-way ANOVA was used to evaluate effects of Area and Animal on the TRT and TRD values. There was a significant main effect of Area ($P < 0.008$), indicating difference in the TRT values between A36 and TE. Neither a main effect of Animal ($P > 0.8$) nor an interaction between Area and Animal ($P > 0.35$) were significant, which assured across-animal consistency in the TRT values. In the case of TRD, there were neither main effects (Area, $P > 0.75$; Animal, $P > 0.70$) nor an interaction ($P > 0.23$).
33. D. J. Amit, N. Brunel, M. V. Tsodyks, *J. Neurosci.* **14**, 6435 (1994).
34. S. Higuchi, Y. Miyashita, *Proc. Natl. Acad. Sci. U.S.A.* **93**, 739 (1996).
35. E. A. Buffalo *et al.*, *Learn. Mem.* **6**, 572 (1999).
36. M. J. Buckley, D. Gaffan, E. A. Murray, *J. Neurophysiol.* **77**, 587 (1997).
37. H. Tomita *et al.*, *Nature* **401**, 699 (1999).
38. I. Hasegawa *et al.*, *Science* **281**, 814 (1998).
39. Experiments were conducted in accordance with the NIH Guide for the Care and Use of Laboratory Animals and with the regulations of the National Institute for Physiological Sciences, Japan. This work was supported by a Grant-in-Aid for Specially Promoted Research (07102006) to Y.M. and by a Grant-in-Aid for Encouragement of Young Scientists (09780744) to Y.N. from the Japanese Ministry of Education, Science, Sports and Culture. We thank A. Ito and S. Shibata for technical assistance and T. Isa, H. Komatsu, S. Mori, K. Ohki, and H. Okuno for discussions.

15 August 2000; accepted 18 December 2000

Glycolipid Antigen Processing for Presentation by CD1d Molecules

Theodore I. Prigozy,[1] Olga Naidenko,[1] Pankaj Qasba,[2] Dirk Elewaut,[1] Laurent Brossay,[1]* Archana Khurana,[1] Takenori Natori,[3] Yasuhiko Koezuka,[3] Ashok Kulkarni,[4] Mitchell Kronenberg[1]†

The requirement for processing glycolipid antigens in T cell recognition was examined with mouse CD1d-mediated responses to glycosphingolipids (GSLs). Although some disaccharide GSL antigens can be recognized without processing, the responses to three other antigens, including the disaccharide GSL Gal(α1→2)GalCer (Gal, galactose; GalCer, galactosylceramide), required removal of the terminal sugars to permit interaction with the T cell receptor. A lysosomal enzyme, α-galactosidase A, was responsible for the processing of Gal(α1→2)GalCer to generate the antigenic monosaccharide epitope. These data demonstrate a carbohydrate antigen processing system analogous to that used for peptides and an ability of T cells to recognize processed fragments of complex glycolipids.

T cells typically recognize peptide antigens presented by major histocompatibility complex–encoded class I or class II molecules. These peptides are generated from well-characterized pathways of protein antigen processing (*1, 2*). T cells that recognize microbial glycolipids in the context of CD1 molecules play a role in host defense (*3, 4*). Additionally, many T cells are reactive with autologous lipids presented by CD1 molecules (*5, 6*). These cells could be important for regulating immune responses and preventing autoimmune disease (*7*). Despite the significance of this antigen recognition system, there is little information on the transport and generation of glycolipids for CD1 presentation.

To determine if carbohydrates can be processed for antigen presentation, we investigated the CD1d-mediated recognition of glycosphingolipids (GSLs). α-Galactosylceramide (α-GalCer) (Fig. 1A) is a GSL isolated from a marine sponge in a screen for anti-metastatic compounds (*8*). It is distinguished from other natural GSLs by the α anomeric linkage of the sugar to the lipid. The cells that respond to α-GalCer presented by CD1d are a separate T cell lineage known as natural killer (NK) T cells (*9, 10*).

We analyzed the response to two closely related α-GalCer analogs, Gal(α1→2)Gal(α1→1)Cer [or Gal(α1→2)GalCer] and Gal(α1→6)GalCer (Fig. 1A). An antigen-presenting cell (APC)–free T cell stimulation assay was used to test the possibility that presentation of these antigens requires internalization and processing (*11, 12*). Although α-GalCer and Gal(α1→6)GalCer bound to mouse CD1d–coated plates could stimulate interleukin-2 (IL-2) release by NK T cell hybridomas, Gal(α1→2)GalCer could not (Fig. 1B). This

[1]Division of Developmental Immunology, La Jolla Institute for Allergy and Immunology, 10355 Science Center Drive, San Diego, CA 92121, USA. [2]Developmental and Metabolic Neurology Branch, National Institute of Neurological Disorders and Stroke, National Institutes of Health, Bethesda, MD 20892, USA. [3]Pharmaceutical Research Laboratory, Kirin Brewery, Gunma 370-12, Japan. [4]Functional Genomics Unit, National Institute of Dental and Craniofacial Research, Bethesda, MD 20892, USA.

*Present address: Department of Molecular Microbiology and Immunology, Brown University, Providence, RI 02912, USA.

†To whom correspondence should be addressed. E-mail: mitch@liai.org